JOURNAL OF GEOPHYSICAL RESEARCH, VOL. 114, D20304, doi:10.1029/2009JD011937, 2009

Overview and characterization of retrievals of temperature, pressure, and atmospheric constituents from the High Resolution Dynamics Limb Sounder (HIRDLS) measurements

Rashid Khosravi,[1] Alyn Lambert,[1,2] Hyunah Lee,[1,3] John Gille,[1,4] John Barnett,[5] Gene Francis,[1] David Edwards,[1] Chris Halvorson,[1] Steve Massie,[1] Cheryl Craig,[1] Charles Krinsky,[4] Joe McInerney,[1] Ken Stone,[1,6] Thomas Eden,[1,7] Bruno Nardi,[1] Christopher Hepplewhite,[5] William Mankin,[1,8] and Michael Coffey[1]

Received 18 February 2009; revised 22 April 2009; accepted 26 June 2009; published 23 October 2009.

[1] The retrieval algorithm for the High Resolution Dynamics Limb Sounder (HIRDLS) instrument onboard NASA's Earth Observing System (EOS) Aura satellite is presented. The algorithm is based on optimal estimation theory, using a modified Levenberg-Marquardt approach for the iterative solution. Overview of the retrieval scheme, convergence criteria, and the forward models is given. Treatments of clouds and aerosols as well as line-of-sight gradients in temperature are described. The retrievals are characterized by high vertical resolution of 1 km and negligible a priori contribution for all products in regions of high signal-to-noise ratio (SNR) (most of the retrieval ranges). It is shown that these characteristics hold for all latitudes along a HIRDLS orbit. The weighting functions are narrow and show good sensitivity to temperature or gas perturbations in regions of high SNR. The retrieval error predicted by the algorithm consists of radiometric noise, pointing jitter error, smoothing error, and forward model error. For temperature, these components are shown for a midlatitude profile as well as for a full orbit. The predicted temperature error varies from 0.5 K to 0.8 K from the upper troposphere to the stratopause region, consistent with the empirical estimates given by Gille et al. (2008). For O_3 and HNO_3, the predicted errors and their useful pressure ranges are, respectively, 10–5% from 50 to 1 hPa and 5–10% from 100 to 10 hPa. These results are based on version V004 of the retrieved data, released in August 2008 to the Goddard Earth Sciences Data and Information Services Center (http://daac.gsfc.nasa.gov).

Citation: Khosravi, R., et al. (2009), Overview and characterization of retrievals of temperature, pressure, and atmospheric constituents from the High Resolution Dynamics Limb Sounder (HIRDLS) measurements, *J. Geophys. Res.*, *114*, D20304, doi:10.1029/2009JD011937.

1. Introduction

[2] The High Resolution Dynamics Limb Sounder (HIRDLS) instrument is an infrared limb-scanning radiometer onboard NASA's Aura satellite, launched on 15 July 2004 in a Sun-synchronous polar orbit (705-km average equator crossing altitude, 98° inclination, and 13:45 ± 15 min local equator crossing time [*Schoeberl et al.*, 2006]). The instrument's goal is to measure atmospheric limb emissions from 6.12 to 17.76 μm in 21 spectral channels to obtain vertical profiles of temperature, pressure, mixing ratios of H_2O, O_3, NO_2, CH_4, N_2O, $ClONO_2$, N_2O_5, HNO_3, CFC-11, CFC-12, and aerosol extinction, as well as cloud top pressures.

[3] HIRDLS was designed to sound the upper troposphere, stratosphere, and lower mesosphere with high vertical and horizontal resolution, obtaining global coverage (including the poles) during both day and night [*Gille et al.*, 2008, 2003]. The design incorporates a two-axis scan mirror to obtain across-track (longitudinal) resolution of approximately 5° at the equator (~500 km) between vertical profiles. The high vertical resolution (~1 km) is achieved by continuously scanning a 1.2-km vertical field of view (FOV) and oversampling the radiance profiles every 0.2 km.

[4] These features represented much improved capabilities over previous limb scanners such as the Limb Infrared Monitor of the Stratosphere (LIMS) [*Gille and Russell*, 1984], and the Improved Stratospheric and Mesospheric Sounder (ISAMS) [*Rodgers et al.*, 1996]. However, the

[1]Atmospheric Chemistry Division, National Center for Atmospheric Research, Boulder, Colorado, USA.
[2]Now at Jet Propulsion Laboratory, California Institute of Technology, Pasadena, California, USA.
[3]Deceased 6 July 2007.
[4]Center for Limb Atmospheric Sounding, University of Colorado at Boulder, Boulder, Colorado, USA.
[5]Department of Physics, University of Oxford, Oxford, UK.
[6]Now at ERT Corporation, Aurora, Colorado, USA.
[7]Now at Computational Physics, Inc., Boulder, Colorado, USA.
[8]Retired.

0148-0227/09/2009JD011937$09.00

instrument's capability to scan across track was lost during decompression at launch, when (apparently) a piece of insulating material detached from inside the instrument housing and covered most of the scan mirror [*Gille et al.*, 2008]. Thus, the radiance scans, which have retained their high vertical resolution, are obtained at a fixed azimuth angle, 47° from the negative velocity vector, on the side away from the Sun. (Note that HIRDLS looks backward relative to the velocity vector.)

[5] The blockage has contaminated the optical beam received at the detectors with its own signal, to varying degree. Depending on a channel's location on the focal plane and the scan mirror's elevation angle, the beam is obscured by ~80–98%. However, on the basis of characterizing the emission from the blockage, algorithms have been designed and implemented in the HIRDLS Level-1 software to correct the measured radiances for the interfering signal. Through these correction algorithms, the retrievals of T, O_3, HNO_3, CFC-11, CFC-12, cloud top pressures, and aerosol extinction at 12.1 μm have improved to the extent that these products have been validated, released, and used in scientific studies [*Gille et al.*, 2008; *Massie et al.*, 2007; *Nardi et al.*, 2008; *Coffey et al.*, 2008; *Kinnison et al.*, 2008; *Alexander et al.*, 2008; *Olsen et al.*, 2008]. As of this writing (June 2009), the latest version of these data is V004 (internally v2.04.19), which is the basis of the results and illustrations in this paper and is available from the Goddard Earth Sciences Data and Information Services Center (GES DISC) (http://daac.gsfc.nasa.gov).

[6] The impact of the blockage on HIRDLS radiances and the correction scheme to remove its contribution to the measured signal is described by *Gille et al.* [2008]. The focus of this paper is on the retrieval algorithm, where the main effects of the obstruction have been on the use of the forward models (section 2.4) and on the approach for correction of line-of-sight (LOS) gradients in temperature and constituent mixing ratios (section 3.4).

[7] The paper is organized as follows. In section 2, the mathematical description of the algorithm is presented. An overview of key retrieval and instrument aspects, such as the sounding channels, retrieval scheme, and treatment of LOS gradients is given in section 3. This is followed by characterization of the retrievals in section 4 and error analysis in section 5. A summary is presented in section 6.

2. Retrieval Algorithm

2.1. Mathematical Description and Solution Method

[8] The HIRDLS retrieval algorithm is based on the optimal estimation solution technique for inverse problems [*Rodgers*, 1976, 1990, 2000]. The objective of this approach is to obtain vertical profiles of atmospheric constituents, for which the algorithm's (forward) radiative transfer model calculates radiances that are consistent with those observed. This is achieved by constructing a scalar cost function, $\Phi(\mathbf{x})$, given by

$$\Phi(\mathbf{x}) = (\mathbf{x}-\mathbf{x}_a)^{\mathbf{T}}\mathbf{S}_a^{-1}(\mathbf{x}-\mathbf{x}_a) + [\mathbf{y}-\mathbf{f}(\mathbf{x})]^{\mathbf{T}}\mathbf{S}_y^{-1}[\mathbf{y}-\mathbf{f}(\mathbf{x})], \quad (1)$$

where $\mathbf{x}$ is the state vector of size N that contains the vertical profiles of all products to be retrieved, $\mathbf{x}_a$ is the a priori state vector having identical structure as $\mathbf{x}$ and representing the prior knowledge of the atmospheric state, $\mathbf{S}_a$ is the N × N a priori error covariance matrix, $\mathbf{y}$ is the measurement vector of size M that consists of the vertical profiles of the observed radiances in all channels, $\mathbf{S}_y$ is the M × M covariance matrix of measurement noise (diagonal for HIRDLS), and $\mathbf{f}(\mathbf{x})$ is the vector of radiances calculated by the forward model, based on the current state of the atmosphere given by $\mathbf{x}$, and having structure identical to $\mathbf{y}$.

[9] The first term in equation (1), the penalty function, constrains the solution to the prior knowledge of the atmosphere, weighted by the a priori uncertainties. The second term, the χ^2 statistics, evaluates the "distance" between the measured and calculated radiances and provides the observational constraint on the retrieved state, weighted by the measurement errors. The maximum a posteriori (MAP) solution is obtained by minimizing equation (1) with respect to $\mathbf{x}$ and solving the resulting equation numerically [*Rodgers*, 2000].

[10] If the system is weakly or moderately nonlinear and the initial guess for the state vector is close to the solution, a Newtonian iteration scheme can be used. However, if the system is strongly nonlinear or the initial guess is far from the solution, the method of steepest descent is more appropriate. For HIRDLS retrievals, the Levenberg-Marquardt approach [*Lambert et al.*, 1999; *Rodgers*, 2000; *Bowman et al.*, 2006], which covers both cases, is adopted. This yields the following iteration equation, which is the basis of the HIRDLS retrieval algorithm:

$$\mathbf{x}_{i+1} = \mathbf{x}_i + \left[(1+\gamma)\mathbf{S}_a^{-1} + \mathbf{K}_i^{\mathbf{T}}\mathbf{S}_y^{-1}\mathbf{K}_i\right]^{-1} \cdot \left\{\mathbf{K}_i^{\mathbf{T}}\mathbf{S}_y^{-1}[\mathbf{y}-\mathbf{f}(\mathbf{x}_i)] - \mathbf{S}_a^{-1}(\mathbf{x}_i-\mathbf{x}_a)\right\}, \quad (2)$$

where i is the iteration count, γ is the step size parameter, and $\mathbf{K} = \frac{\partial \mathbf{f}(\mathbf{x})}{\partial \mathbf{x}}$ is the weighting function matrix (M × N), which represents the sensitivity of the forward model to perturbations in the state vector (section 4.2). To solve this equation efficiently, it is cast into the form of a set of simultaneous equations that are solved by using the methods of linear algebra,

$$\mathbf{M}\ \delta\mathbf{x} = \mathbf{b}, \quad (3)$$

where $\mathbf{M} \equiv (1+\gamma)\mathbf{S}_a^{-1} + \mathbf{K}_i^{\mathbf{T}}\mathbf{S}_y^{-1}\mathbf{K}_i$ is an N × N symmetric, positive definite matrix, $\delta\mathbf{x} \equiv \mathbf{x}_{i+1} - \mathbf{x}_i$ is the solution increment vector of size N, and $\mathbf{b} \equiv \mathbf{K}_i^{\mathbf{T}}\mathbf{S}_y^{-1}[\mathbf{y} - \mathbf{f}(\mathbf{x}_i)] - \mathbf{S}_a^{-1}(\mathbf{x}_i - \mathbf{x}_a)$ is a vector of size N.

[11] Note that because of the wide range of values of volume mixing ratios (VMR) of the trace gas products (e.g., H_2O, O_3), ln(VMR) is used in the state vector to obtain more accurate retrievals [*Rodgers*, 2000; *Deeter et al.*, 2007].

2.2. Trust Region and Determination of γ

[12] The general criterion for updating γ is to increase it and reject $\mathbf{x}_{i+1}$ if $\Phi(\mathbf{x}_{i+1}) > \Phi(\mathbf{x}_i)$, and to decrease it and accept $\mathbf{x}_{i+1}$ if $\Phi(\mathbf{x}_{i+1}) < \Phi(\mathbf{x}_i)$. A more efficient scheme is implemented in the HIRDLS retrieval algorithm, which combines the general criterion with a simplified "trust region" approach [*Rodgers*, 2000]. In this scheme, γ is updated on the basis of the ratio of the change in the actual cost function to

that calculated using a linear approximation to the forward model,

$$R = \frac{\Phi(\mathbf{x}_i) - \Phi(\mathbf{x}_{i+1})}{\Phi(\mathbf{x}_i) - \Phi_L(\mathbf{x}_{i+1})}, \quad (4)$$

where $\Phi_L(\mathbf{x}_{i+1})$ is calculated by using $\mathbf{f}(\mathbf{x}_{i+1}) \approx \mathbf{f}(\mathbf{x}_i) + \mathbf{K}[\mathbf{x}_{i+1} - \mathbf{x}_i]$ in equation (1).

[13] If the estimate of the state vector at iteration i + 1 is close to the solution, then $\Phi_L(\mathbf{x}_{i+1}) \approx \Phi(\mathbf{x}_{i+1})$ and R $\approx$ 1. In contrast, if $\mathbf{x}_{i+1}$ is far away from the solution, then R is close to 0 (or negative). Therefore, there is a "trust region," within which $\mathbf{x}_{i+1}$ is an acceptable iterate. This region is bounded by $R_{min} = \frac{1}{4}$ and $R_{max} = \frac{3}{4}$ [*Rodgers*, 2000], so that: (1) if $R < R_{min}$, $\mathbf{x}_{i+1}$ is probably far from the solution, it is rejected, and $\gamma \rightarrow 10\gamma$; (2) if $R > R_{max}$, $\mathbf{x}_{i+1}$ is probably close to the solution, it is accepted, and $\gamma \rightarrow \frac{1}{10}\gamma$; (3) otherwise, $\mathbf{x}_{i+1}$ is in the trust region, it is accepted and γ is unchanged.

2.3. Convergence

[14] The general guidelines for stopping the iteration loop are as follows: (1) prevent overrunning the loop, which would waste computational resources and degrade performance; (2) prevent underrunning the loop so as not to stop short of the optimal solution; and (3) terminate ill-behaved retrievals that do not converge.

[15] The first two criteria are implemented by requiring that the difference between the current and the last iterates, $\mathbf{x}_{i+1} - \mathbf{x}_i$, weighted by the calculated covariance, $\mathbf{S}_x$, be less than a predefined convergence parameter, ε, scaled by the number of elements in the state vector (N); i.e.,

$$(\mathbf{x}_{i+1} - \mathbf{x}_i)^T \mathbf{S}_x^{-1} (\mathbf{x}_{i+1} - \mathbf{x}_i) < \varepsilon N, \quad (5)$$

where $\mathbf{S}_x$ is given by equation (7). The last criterion is implemented by limiting the number of iterations. For V004 of HIRDLS data, the values of ε and maximum iteration number, optimized after many test runs of the algorithm, are 0.1 and 20, respectively.

2.4. Forward Models

[16] Two forward models, FM1 and FM2 [*Francis et al.*, 2006], are used in the current version of HIRDLS operational processing (V004). FM1 is based on Curtis-Godson (CG) and emissivity-growth (EG) approximations [*Curtis*, 1952; *Weinreb and Neuendorffer*, 1973], and depending on channel and tangent height achieves radiance accuracy of 1–5% relative to line-by-line calculations based on GENLN-3 [*Edwards*, 1992]. FM2 was developed to achieve the high accuracy and performance requirements imposed by the prelaunch instrument design specifications. It combines the CG and EG framework of FM1 with a physically based statistical regression model to yield radiances having accuracy of 0.5–1.0% relative to GENLN-3.

[17] One impact of the obstruction on the retrievals has been on the use of the HIRDLS forward models. Prior to launch, the retrievals were set up to be run in one pass using FM2. However, because of contamination of the radiances with the blockage signal, temperature and mixing ratio profiles obtained during the retrieval iteration are too noisy to take direct advantage of the accuracy of FM2 in one pass. Therefore, the retrievals are performed in two passes. In the first stage, FM1 is used to obtain inversions that are near the optimal solution. These retrievals are then passed as initial guess to the second stage, which employs FM2 to obtain the final solution. This scheme yields more accurate retrievals and reduces the number of diverged profiles.

2.5. Algorithm Testing

[18] A series of tests are performed with every build of the HIRDLS Level-2 software (L2) to verify the correctness of changes in the results due to any algorithm or software modifications, and to help diagnose and prevent anomalous retrievals. Among these is a consistency test, designed to evaluate the accuracy of the retrievals when the input radiances are "perfect," i.e., noise free. The radiances for these tests are simulated by the forward model based on a "truth" climatology consisting of model and/or independently measured data. In the subsequent retrieval step using these radiances, the same sources for temperature/pressure and mixing ratios of channel contaminants are used as in the simulation. Also, these retrievals are performed using the same error sources as in the operational processing (section 5); i.e., measurement, a priori, and forward model. The retrievals in these tests show very close agreement with the "truth" climatology. For example, the absolute value of the deviations are $\leq$0.5 K for temperature, and $\leq$2% for the trace gases in most of the retrieval regions.

3. Key Retrieval Aspects

3.1. Sounding Channels

[19] The 21 spectral channels of HIRDLS were selected on the basis of spectral and radiative transfer modeling [*Edwards et al.*, 1995], with the objectives of maximizing the signal-to-noise ratio for the target gases, avoiding or minimizing interfering signals from contaminating species, and characterizing contamination with the aid of the other channels. Optimizing these criteria has yielded the channel configuration given in Table 1. The 50% filter response values were obtained during instrument calibration (T. Eden Jr. et al., Spectral characterization of the HIRDLS flight instrument from pre-launch calibration data, submitted to *IEEE Transactions on Geoscience and Remote Sensing*, 2009), and generally fall within the specified requirements [*Lambert et al.*, 1999]. The radiometric (measurement) noise values are higher than the prelaunch specifications by about 1.1 to 2.7 times (depending on channel), reflecting the increased noise level due to the obstruction of the scan mirror.

[20] The sounding range given in Table 1 for each channel represents an estimate of tangent heights over which useful retrievals could have been obtained without the blockage. However, the presence of the blockage has resulted in lower levels for the retrieval top, which in the current (V004) operational processing correspond to tangent heights above which channel radiances are too contaminated with the blockage signal (noise).

[21] Channels 4 and 5 (temperature), 11 (O_3), and 20 (H_2O) were designed to sound higher altitudes in the atmosphere than their companion channels by situating their spectral response curves in the high optical depth regions of the CO_2, O_3, and H_2O spectra, respectively [*Edwards et al.*, 1995]. The lower retrieval limits for these channels have been extended

Table 1. Characteristics of HIRDLS Sounding Channels

Channel	Target Species[a]	50% Response (cm^{-1}) Lower	50% Response (cm^{-1}) Upper	Sounding Range (km)	Retrieval Range (km)	Radiometric Noise (10^{-4} W/m^2/sr)
1	Aerosol	566.87	584.29	8–70	7–32	20.18
2	T, P (L)	599.82	615.11	8–60	7–65	6.69
3	T, P (M)	612.06	636.52	8–60	7–65	6.78
4	T, P (M)	629.44	652.73	15–60	7–65	7.29
5	T, P (H)	657.09	680.81	30–105	7–65	4.19
6	Aerosol	819.89	834.94	8–55	7–32	4.58
7	CFC11	834.61	850.64	8–50	7–44	4.17
8	HNO_3	861.96	900.82	8–70	7–44	6.16
9	CFC12	915.59	931.99	8–50	7–44	2.68
10	O_3 (M)	991.79	1008.49	8–55	7–60	2.77
11	O_3 (H)	1013.69	1043.96	30–85	7–65	2.61
12	O_3 (L)	1120.41	1139.69	8–55	7–55	1.79
13	Aerosol	1202.61	1221.42	8–55	7–32	1.74
14	N_2O_5	1230.47	1257.60	8–60	7–44	2.22
15	N_2O	1255.93	1278.48	8–70	7–44	2.50
16	$ClONO_2$	1279.19	1299.48	8–70	7–44	1.85
17	CH_4	1327.04	1366.05	8–80	7–44	2.72
18	H_2O (M)	1386.95	1432.21	8–40	7–55	2.02
19	Aerosol	1401.38	1415.50	8–55	7–32	1.74
20	H_2O (H)	1428.38	1532.57	15–85	7–55	4.32
21	NO_2	1585.19	1632.92	8–70	7–52	1.96

[a]L, M, and H next to some target gases denote low-, medium-, and high-altitude sounding ranges for the corresponding channel.

downward to increase the measurement contribution as much as possible.

[22] Table 2 shows the absorbers that contribute to each channel's total radiance. These are distinguished as primary products, jointly retrieved products, and contaminants, which are gases whose contributions to the total radiance in a channel are significant but are not retrieved. Jointly retrieved products are target gases that have relatively strong signal in a channel's spectral band and are retrieved simultaneously with the primary product. For example, channels 14, 15, 16, and 17, having a combined band pass of 1210–1400 cm^{-1}, were designed to retrieve N_2O_5, N_2O, $ClONO_2$, and CH_4, respectively. However, since the spectra of these gases overlap in this band pass, these channels cannot be considered as independent and the four gases are therefore retrieved simultaneously in one step using all four channels. Similarly, CFC-11, HNO_3, and CFC-12 are jointly retrieved in channels 7, 8, and 9. Note that channel 9 is also used in a separate step to retrieve aerosol extinction in the spectral band, 910–940 cm^{-1}.

3.2. Retrieval Scheme and Supporting Data

[23] Before launch, various retrieval schemes were investigated to optimize accuracy and processing performance. These schemes included simultaneous retrieval of all products in one step, multistep retrievals with feedback of a retrieved gas profile to a subsequent step as a contaminant, and applying line-of-sight gradient correction for both tem-

Table 2. Identification of Primary Products and Contaminants in the HIRDLS Sounding Channels

Channel	Primary Product	Contaminants and Products Retrieved Jointly[a]
1	Aerosol 17.4 μm	CO_2, H_2O, O_3, N_2O, N_2O_5
2	T, P	H_2O, O_3, N_2O, N_2O_5, Aerosol
3	T, P	H_2O, O_3, N_2O, Aerosol
4	T, P	H_2O, O_3, N_2O, Aerosol
5	T, P	H_2O, O_3, Aerosol
6	Aerosol 12.1 μm	CO_2, H_2O, O_3, NO_2, HNO_3, CFC11, $ClONO_2$
7	CFC11	CFC12 (J), HNO_3 (J), CO_2, H_2O, O_3, NO_2, $ClONO_2$, Aerosol,
8	HNO_3	CFC11 (J), CFC12 (J), CO_2, H_2O, O_3, NO_2, Aerosol
9	CFC12	CFC11 (J), HNO_3 (J), CO_2, H_2O, O_3, NO_2, N_2O, Aerosol
9	Aerosol 10.8 μm	CO_2, H_2O, O_3, NO_2, N_2O
10	O_3	CO_2, H_2O, Aerosol
11	O_3	CO_2, H_2O, Aerosol
12	O_3	CO_2, H_2O, N_2O, CFC12, CH_4, Aerosol
13	Aerosol 8.3 μm	CO_2, H_2O, O_3, N_2O, CH_4, N_2O_5
14	N_2O_5	N_2O (J), $ClONO_2$ (J), CH_4 (J), HNO_3, CO_2, H_2O, O_3, Aerosol
15	N_2O	N_2O_5 (J), $ClONO_2$ (J), CH_4 (J), HNO_3, CO_2, H_2O, Aerosol
16	$ClONO_2$	N_2O_5 (J), N_2O (J), CH_4 (J), HNO_3, CO_2, H_2O, Aerosol
17	CH_4	N_2O_5 (J), N_2O (J), $ClONO_2$ (J), HNO_3, CO_2, H_2O, Aerosol
18	H_2O	CO_2, CH_4, O_2, Aerosol
19	Aerosol 7.1 μm	CO_2, H_2O, CH_4
20	H_2O	CO_2, CH_4, O_2, Aerosol
21	NO_2	CO_2, H_2O, CH_4, O_2, Aerosol

[a]J denotes gases that are retrieved jointly with the primary gas (see text).

Table 3. Construction of Covariance Matrices for the Error Sources in the HIRDLS Retrieval Algorithm V004[a]

Error Covariance	Diagonal Elements	Off-Diagonal Elements
a priori ($\mathbf{S}_a$)	$(20\ K)^2$ ... temperature $(0.75)^2$ ... pressure $(3)^2$ ... trace gases $(10)^2$ ... aerosol extinction	$\sqrt{\mathbf{S}_a^{ii}\mathbf{S}_a^{jj}}\exp(-\lvert z_i - z_j\rvert/l)$
Forward Model ($\mathbf{S}_{f'}$)	$(0.3\% * \text{Forward Model Rad})^2$	0
Measurement ($\mathbf{S}_y$)	$(\text{Radiometric Detector Noise})^2 + (\text{Pointing Jitter Noise})^2$	0

[a]For $\mathbf{S}_a$, the diagonal elements represent the variances of the a priori data (square of the standard deviations). For pressure, trace gases, and aerosol extinction, the a priori errors are constructed so as to give the stated standard deviations relative to the a priori data. For example, for an a priori ozone mixing ratio of 6 ppmv, the corresponding error is constructed to be 18 ppmv, yielding a standard deviation of 3 (300%). Large values are selected for the diagonal elements to allow the retrieval ample freedom to arrive at a solution dominated by the observed radiances. For the off-diagonal elements, l is the covariance length, taken to be 5 km for T and trace gases and 1 km for aerosol extinction. Detector noise is based on calibration data (T. Eden Jr. et al., Radiometric calibration of the HIRDLS flight instrument from pre-launch calibration data, submitted to *IEEE Transactions on Geoscience and Remote Sensing*, 2009), scaled by the unobstructed area of the aperture.

perature and gas retrievals (see section 3.4). In the current operational processing, retrieval of the complete suite of products is performed in sequential steps, beginning with temperature and pressure (T/P). This is followed by retrievals of H_2O, O_3, NO_2, the group of N_2O, N_2O_5, $ClONO_2$, and CH_4, the group of CFC-11, HNO_3, and CFC-12, and aerosol extinction at 17.4, 12.1, 10.8, 8.3, and 7.1 μm (midband wavelengths of channels 1, 6, 9, 13, and 19). Gas and extinction retrievals are performed using the retrieved T/P from the first step. In version 4 of HIRDLS data, the retrievals of T/P, H_2O, and O_3 from the first pass through the iteration loop are used as initial guess in the second pass to obtain more accurate results (section 2.4).

[24] Temperature and pressure retrievals are performed jointly (section 3.3) using Global Modeling and Assimilation Office (GMAO) Goddard Earth Observing System (GEOS) (see http://gmao.gsfc.nasa.gov) data for initial guess and LOS gradient correction. GEOS-5 version 5.0.1 analyses data are used for HIRDLS V004 retrievals. T/P a priori profiles are constructed by geolocating to HIRDLS tangent heights Committee on Space Research (COSPAR) International Reference Atmosphere (CIRA) [*Fleming et al.*, 1990] data.

[25] Retrievals of gas mixing ratios are performed using "climatology" data for initial guess, a priori, and contaminants. This data set is constructed by geolocating to HIRDLS tangent heights monthly mean gas mixing ratios from the NCAR 3-D chemical transport model, MOZART (Model for Ozone And Related chemical Tracers) [*Kinnison et al.*, 2007]. The climatology data set is also used for the contaminants in the temperature channels. The a priori covariance matrix is constructed according to Table 3 (see also section 5).

3.3. Pressure Retrieval

[26] Pressure profiles, $P(z)$, are obtained by jointly retrieving with temperature, the pressure P_0 corresponding to a reference altitude z_0 (30 km in V004), and then integrating the hydrostatic equation using the retrieved temperature profiles, $T(z)$,

$$\ln(P(z)) = \ln(P_0(z_0)) + \int_{z_0}^{z} \frac{M_r g(\phi, z)}{RT(z)} dz,$$

where R is the gas constant, M_r is the molecular mass of air, and $g(\phi, z)$ is the acceleration due to gravity at latitude ϕ and altitude z.

3.4. Line-of-Sight Gradient Correction

[27] Another impact of the blockage on the retrieval algorithm has been on the method for correction of LOS gradients in T and gas mixing ratios. Because of the loss of capability to scan the atmosphere in longitudinal direction (across track), the prelaunch scheme for LOS gradient correction could not be exercised. This method employed two passes through the retrieval algorithm. In the first pass, the atmospheric field would be considered as homogeneous (no gradients along LOS). The retrieved fields would then be used in the subsequent pass to compute the gradients, which would be applied in the forward model calculations.

[28] In the current scheme, LOS gradient correction is performed only for temperature, using GMAO/GEOS (section 3.2) data collocated to points along the LOS. Temperature gradients are calculated and applied in the forward model as before. The retrieved T/P profiles are then used for the subsequent gas retrievals, where LOS temperature gradients are again applied to calculate transmittances accurately.

3.5. Treatment of Aerosols and Clouds

[29] Aerosols and clouds absorb atmospheric infrared radiation, and hence affect radiance data measured by satellite remote sensing. Aerosol opacity varies gradually with wavelength (in contrast to gaseous opacity), and is a significant component of atmospheric infrared optical depth, particularly after volcanic eruptions. Therefore, inversion of radiance data must account for aerosol absorption.

[30] HIRDLS retrievals incorporate aerosols in two ways. Background sulfate aerosols are included as contaminating absorbers in all channels. Extinction profiles for these aerosols are calculated by a spectral model [*Livingston and Russell*, 1989; *Carslaw et al.*, 1995] that uses the radiance data in the most sensitive aerosol channel (6) as reference.

[31] In addition to correcting for their interfering signals as contaminants, vertical profiles of aerosol extinction are retrieved using radiances measured in channels 1, 6, 9, 13, and 19, with midband wavelengths of 17.4, 12.1, 10.8, 8.3, and 7.1 μm, respectively. These inversions are performed with the retrieved T/P profiles. Using the spectral model mentioned above, the initial guess and a priori data are constructed by mapping the Stratospheric Aerosol and Gas Experiment II (SAGE-II) [*Russell and McCormick*, 1989] retrievals to the midband wavelengths of the aerosol channels. These SAGE-II data reflect the volcanically quiescent period well after the eruption of Mount Pinatubo. The mixing

ratio profiles of the gas contaminants in the aerosol channels are obtained from the MOZART model data.

[32] In the current operational algorithm, the radiances at and below cloud tops in all channels are excluded from the retrievals to avoid inaccurate solutions. By construct, the optimal estimation method increases the contribution of a priori data in the retrieved profiles in these regions (progressively below cloud tops). The cloud top heights are passed on to the retrieval step by a cloud detection algorithm that is described by *Massie et al.* [2007]. It is based on detecting radiance perturbations in channels 6 and 12 relative to clear-sky conditions. Note also that to account for a detector's finite FOV, it is deconvolved from the observed radiances prior to the retrieval step, thus correcting for possible cloud contamination of the radiances above cloud tops.

4. Retrieval Characterization

4.1. Averaging Kernels

[33] In this section, HIRDLS retrievals, based on observed radiances (V004), are characterized by analyzing the averaging kernel matrix, **A**, calculated using the following expression [*Rodgers*, 2000]:

$$\mathbf{A} = \mathbf{S}_x \mathbf{K}^T \mathbf{S}_y^{-1} \mathbf{K}, \tag{6}$$

where $\mathbf{S_X}$ is the solution error covariance matrix given by

$$\mathbf{S_x} = \left(\mathbf{S_a^{-1}} + \mathbf{K^T S_y^{-1} K}\right)^{-1}, \tag{7}$$

and the other terms are defined in section 2.1. Matrix **A** represents the response of the retrieved state to perturbations of the "true" state,

$$\mathbf{A} = \frac{\partial \mathbf{x}}{\partial \mathbf{x}_t},$$

where $\mathbf{x}_t$ is the state vector of the true atmosphere. Row i of **A**, denoted by $\mathbf{A}_{ij}$, represents the variation of a retrieved quantity with altitude (j) due to a perturbation at level i of the same (or another) quantity in the true atmosphere. For an ideal instrument and retrieval algorithm, $\mathbf{A} = \mathbf{I}$, where **I** is the identity matrix, so that each row of **A** is a delta function whose peak is at the perturbation level, indicating that the retrieved quantity is affected only at that level. For a nonideal system, averaging kernels indicate how the true profiles are smoothed by the instrument FOV and the retrieval algorithm. For example, full width at half maximum (FWHM) of the kernels gives a measure of the vertical resolution of the system. Each kernel also has an area that represents approximately the fraction of the contribution to the retrieval by the observed radiances rather than by the a priori data; that is, the closer the area is to 1 the less the a priori contribution.

[34] Limb viewing instruments with low noise and high vertical resolution can approach the ideal case, having sharply peaked kernels. As shown in Figure 1, HIRDLS is such an instrument. Figure 1 illustrates representative averaging kernels for Temperature, H_2O, O_3, and HNO_3 for retrievals based on a northern hemisphere winter, mid latitude radiance scan (see Figure 1 caption). The kernels are sharply peaked at almost 1 (0.99) and are very narrow, having a FWHM of 1 km at most tangent heights, as shown by the blue curves. Furthermore, the red curves, which consist of points that are the areas of the kernels placed at the perturbation tangent heights, show that HIRDLS retrievals are independent of the a priori in most of the retrieval range. The a priori begins to contribute to the solution at the top most levels, where the signal-to-noise ratio (SNR) weakens, as well as at the bottom most levels, where either the channels become saturated (e.g., temperature channels), the SNR is small (e.g., HNO_3), or clouds are encountered (see sections 3.5 and 4.2). Note also that in regions where the retrievals are independent of the a priori, the averaging kernels peak at the heights where the perturbations occur. Combined with the narrow widths of the kernels in these regions, this indicates that the response of the retrieval is localized at the perturbation level, with almost no smoothing by the a priori. In the lower most regions, however, the retrieval responds at tangent heights higher than the perturbation levels (because of lack of sensitivity), causing the averaging kernels to overlap.

[35] It is important to note that the retrieval characteristics described above for a single profile are maintained for all latitudes along full orbits of HIRDLS observations. This is illustrated in Figures 2 and 3, which show, respectively, curtain plots of the red and blue curves in Figure 1 along a full HIRDLS orbit (for temperature and O_3). Clearly, the retrievals are dominated by the observed radiances and have high vertical resolution for all latitudes along the orbit track for most of the retrieval's vertical range.

4.2. Weighting Functions

[36] Another retrieval diagnostic tool is provided by weighting functions, defined by the matrix $\mathbf{K} = \frac{\partial \mathbf{f}(\mathbf{x})}{\partial \mathbf{x}}$. Each row of **K** represents the response, as a function of altitude, of the radiances calculated by the forward model to a perturbation in temperature or gas mixing ratio at a given tangent height (see caption for Figure 4). The weighting functions, i.e., the rows of **K**, corresponding to the averaging kernels of Figure 1. are plotted in Figures 4, 5, and 6 for the temperature, H_2O, and O_3 sounding channels, respectively.

[37] As shown in Figure 4, the weighting functions for channels 2 and 3 show sensitivity down to ~11 km, and reach maximum response at ~20 km and 26 km, respectively, achieving the design objectives of these channels for high sensitivity at lower altitudes [*Edwards et al.*, 1995]. It can also be seen that, consistent with the radiance profiles for this scan (Figure 7), these channels do not respond to temperature perturbations below ~10 km, i.e., are opaque in that region. As a result, at these lower altitudes in the upper troposphere lower stratosphere (UTLS), the weighting functions peak (and overlap) at altitudes higher than the perturbation tangent heights that are marked by the red dots (see Figure 4 caption). Beginning at about 14 km (channel 2) and 17 km (channel 3), the red dots coincide with the peaks, showing that the maximum radiance response in these channels occurs at the same tangent height as the perturbation height. Moreover, the weighting functions for altitudes above 17 km become narrow, indicating that most of the radiance response comes from the perturbation level, implying good vertical resolution.

[38] Note that for a weighting function whose peak coincides with its red dot, the value at the tangent height

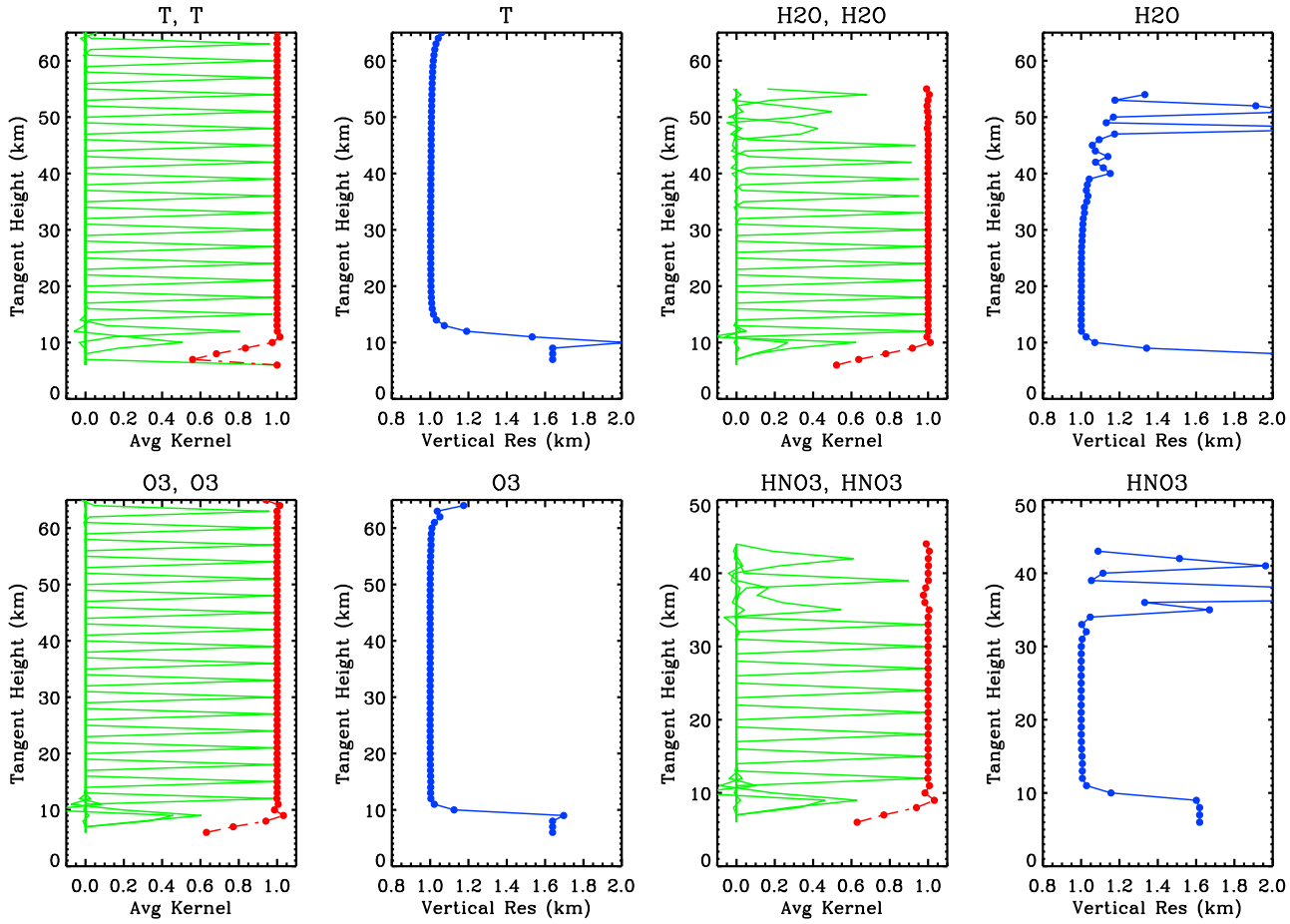

Figure 1. HIRDLS averaging kernels (green curves) and vertical resolution (blue curves) based on an observed radiance scan (V004) for 15 January 2007, at 45.4°N, having a cloud top height of 9 km. Kernels are shown for $\frac{\partial T}{\partial T_t}$, $\frac{\partial O_3}{\partial (O_3)_t}$, $\frac{\partial H_2O}{\partial (H_2O)_t}$, and $\frac{\partial HNO_3}{\partial (HNO_3)_t}$. Every third kernel has been plotted to show clearly that the kernels are sharply peaked and narrow. The red curves give the area under each kernel (plotted at the perturbation tangent heights). Note the change in the altitude scale for HNO_3.

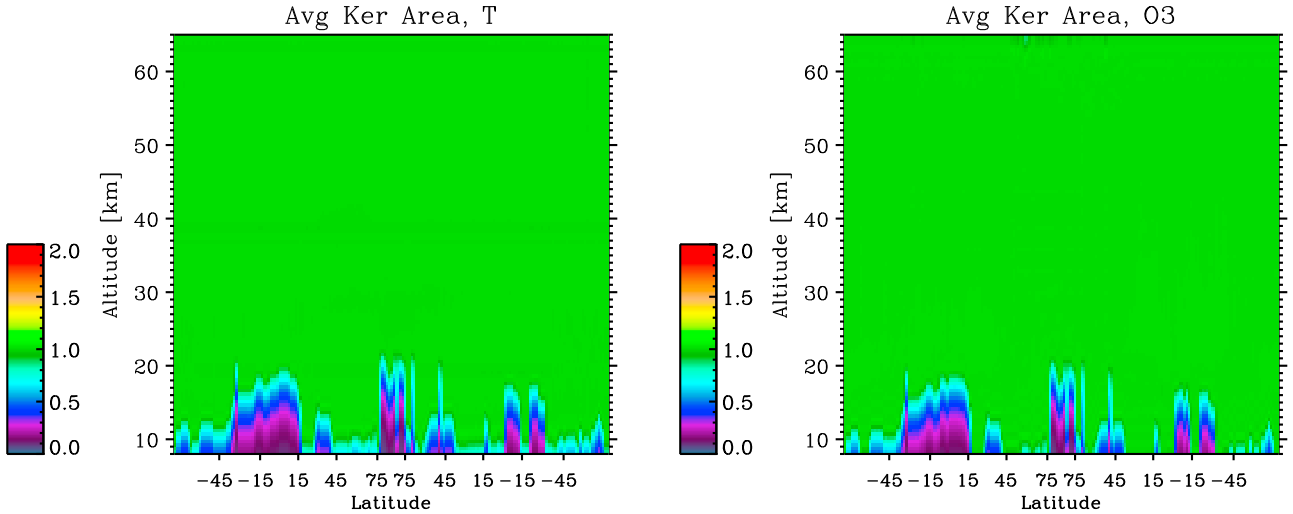

Figure 2. Maps of the area of averaging kernel rows (red curves in Figure 1) along a full orbit of HIRDLS observations for retrieved temperature and O_3 (V004). Each curtain plot is a juxtaposition of the red curves along the observation latitudes of one full HIRDLS orbit on 15 January 2007. The vertical intrusions represent cloudy regions.

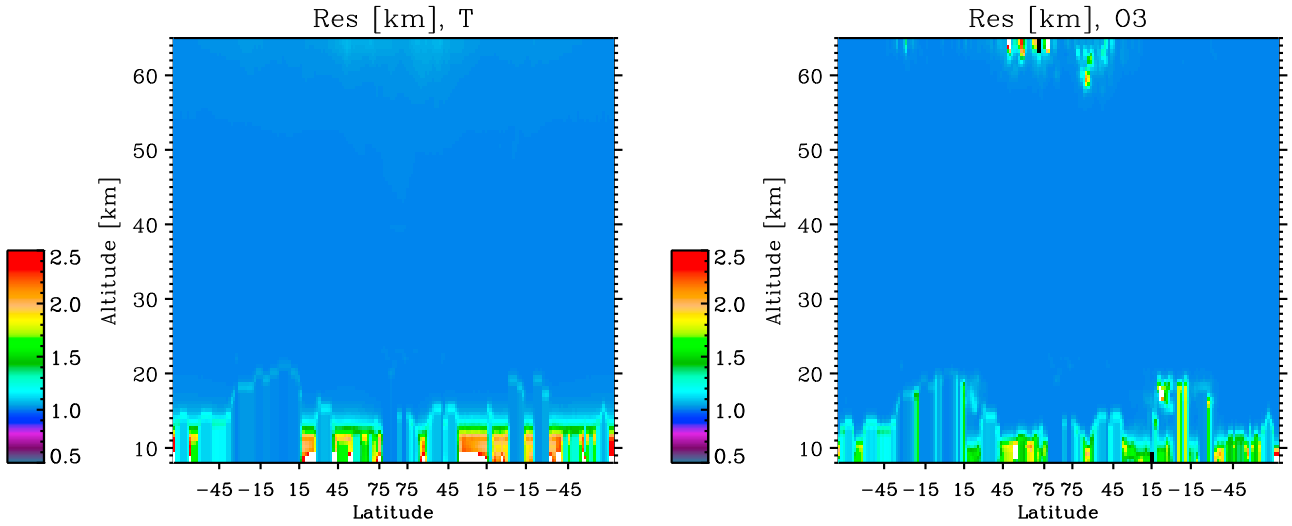

Figure 3. Maps of the vertical resolution (blue curves in Figure 1) along a full orbit of HIRDLS observations for retrieved temperature and O_3 (V004). Each curtain plot is a juxtaposition of the blue curves along the observation latitudes of one full HIRDLS orbit on 15 January 2007.

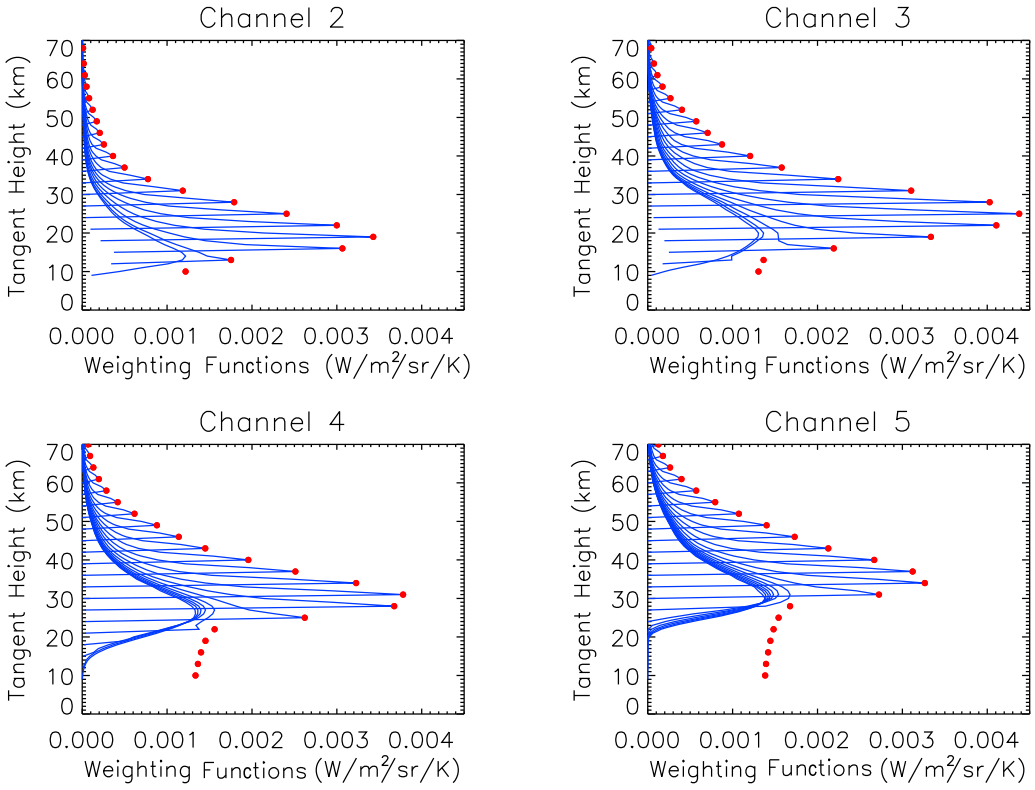

Figure 4. Weighting functions for the HIRDLS temperature sounding channels for the radiance scan used in Figure 1 (V004, 45.4°N). Each curve for channel n ($n = 2, 3, 4, 5$) is a plot of row i of **K** (section 4.2) and shows $\frac{\partial \mathbf{f}_j^n}{\partial T_i}$ as a function of altitude (j) due to a perturbation in temperature at tangent height i (**f** is the forward model radiance and T is temperature). Each weighting function curve has a corresponding red dot, which marks the peak of that curve on the horizontal axis and is placed vertically at the perturbation tangent height of the curve (i). Coincidence of a red dot with the peak of its corresponding curve indicates that the maximum sensitivity of the channel radiance to a temperature perturbation at tangent height i occurs at the same height (i). Every third function is plotted for clarity. Note that when the peaks coincide with the red dots, the weighting functions are not zero immediately below their peaks owing to refraction effects (see section 4.2).

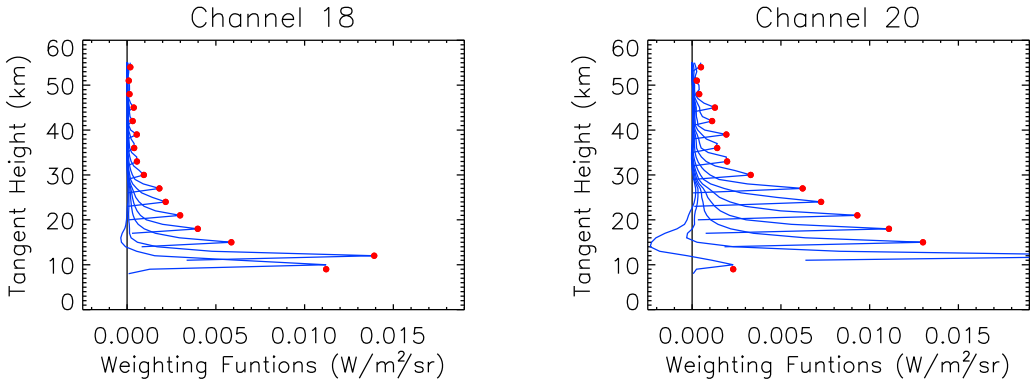

Figure 5. Weighting functions for the HIRDLS water vapor sounding channels. Each curve for channel n (n = 18, 20) is a plot of row i of **K** (section 4.2) and shows $\frac{\partial \mathbf{f}_j^n}{\partial ln(H_2O)_i}$, which is the response of the forward model radiance (**f**) as a function of altitude (j) due to a perturbation in (log of) water vapor volume mixing ratio at tangent height i. See Figure 4 caption for more details.

immediately below the red dot is not zero, although very small (e.g., channel 2 between 10 and 20 km). This is because the tangent heights of the weighting functions (red dots) are plotted on the geometric (and uniform) grid of the retrieval algorithm. The true tangent heights, however, are lower than the geometric ones owing to atmospheric refraction [*Lambert et al.*, 1999], resulting in a (small) radiance response immediately below the plotted perturbation levels (red dots). The weighting functions are zero below these lowest levels, and are not shown. Furthermore, as the red dots move up in altitude, the effect of refraction diminishes, resulting in an exceedingly smaller value of the weighting function at the level immediately below a peak. These near-zero values appear to lie on the vertical axis, but are not exactly zero.

[39] For channels 4 and 5, the weighting functions peak at about 31 km and 34 km, respectively, indicating high channel sensitivity to temperature in the mid to upper stratosphere; these channels are opaque below ~15 km and 21 km, respectively (see also Figure 7). The peaks of the radiance response for channels 4 and 5 begin to coincide with the perturbation heights at about 26 km and 31 km, respectively. Note that these channels retain good sensitivity in the upper stratosphere and lower mesosphere region. This is particularly true of channel 5, which is by design the highest-altitude temperature sounding channel [*Edwards et al.*, 1995].

[40] As mentioned in section 3.5, parts of a radiance scan that pass through clouds are omitted from the **y** vector in the retrieval algorithm (equation (2)), resulting in a progressively larger contribution by the a priori to the retrievals below cloud tops. In these cases, the lower portions of the weighting functions of channels 2, 3, and 4 that peak above their perturbations levels (red dots) could lose sensitivity at higher altitudes than shown in Figure 4, depending on the cloud top height (9 km for the present radiance scan).

[41] The weighting functions for the H_2O and O_3 sounding channels (expressed in terms of the log of volume mixing ratios) are shown in Figures 5 and 6, respectively. For H_2O, the weighting functions of the higher-altitude channel 20 show maximum sensitivity to water vapor at ~12 km, retaining good response and vertical resolution through mid stratosphere. The lower-altitude channel 18 shows good response and vertical resolution down to ~10 km. For O_3, the weighting functions of the higher-altitude channel 11 show peak sensitivity to ozone at about 30 km and retain very good sensitivity throughout the stratosphere. At lower altitudes in the UTLS regions, this channel shows low sensitivity to ozone as indicated by the weighting functions peaking at higher altitudes than the perturbation levels. The weighting functions of the lower-altitude channels 10 and 12 show much stronger sensitivity in the UTLS region than those of channel 11, accomplishing the design objectives of these channels.

5. Retrieval Error Analysis

[42] The predicted retrieval error (identified by the suffix "Precision" added to the product names in the output data files delivered to the GES DISC) consists of contributions by measurement noise, forward model error, model parameter error, and a priori (smoothing) error. This can be seen by regarding the retrieved state (**x**) as a weighted mean of the true ($\mathbf{x}_t$) and a priori ($\mathbf{x}_a$) states with contributions from the error sources just mentioned [*Rodgers*, 2000],

$$\mathbf{x} = \mathbf{A}\mathbf{x}_t + (\mathbf{I} - \mathbf{A})\mathbf{x}_a + \mathbf{G}_y\left[\mathbf{K}_b(\mathbf{b}_t - \mathbf{b}) + \Delta\mathbf{f}(\mathbf{x}_t, \mathbf{b}_t) + \varepsilon_y\right], \tag{8}$$

where $\mathbf{G}_y = \frac{\partial \mathbf{x}}{\partial \mathbf{y}} = (\mathbf{S}_a^{-1} + \mathbf{K}^T\mathbf{S}_y^{-1}\mathbf{K})^{-1}\mathbf{K}^T\mathbf{S}_y^{-1}$ is the gain matrix [*Lambert et al.*, 1999], $\mathbf{K}_b = \frac{\partial \mathbf{f}}{\partial \mathbf{b}}$ is the sensitivity of the forward model radiances to forward model parameters (**b**) and is known as the model parameter matrix, $\Delta\mathbf{f}$ is the forward model error term, and ε_y is the measurement noise. Equation (8) can be rewritten to show the deviation of the retrieved state from the true state in terms of the error sources,

$$\begin{aligned} \mathbf{x} - \mathbf{x}_t = {} & (\mathbf{A} - \mathbf{I})(\mathbf{x}_t - \mathbf{x}_a) && \text{smoothing error} \\ & + \mathbf{G}_y\mathbf{K}_b(\mathbf{b}_t - \mathbf{b}) && \text{model parameter error} \\ & + \mathbf{G}_y\Delta\mathbf{f}(\mathbf{x}_t, \mathbf{b}_t) && \text{forward model error} \\ & + \mathbf{G}_y\varepsilon_y && \text{measurement error} \\ & \equiv \varepsilon_s + \varepsilon_b + \varepsilon_f + \varepsilon_m. \end{aligned} \tag{9}$$

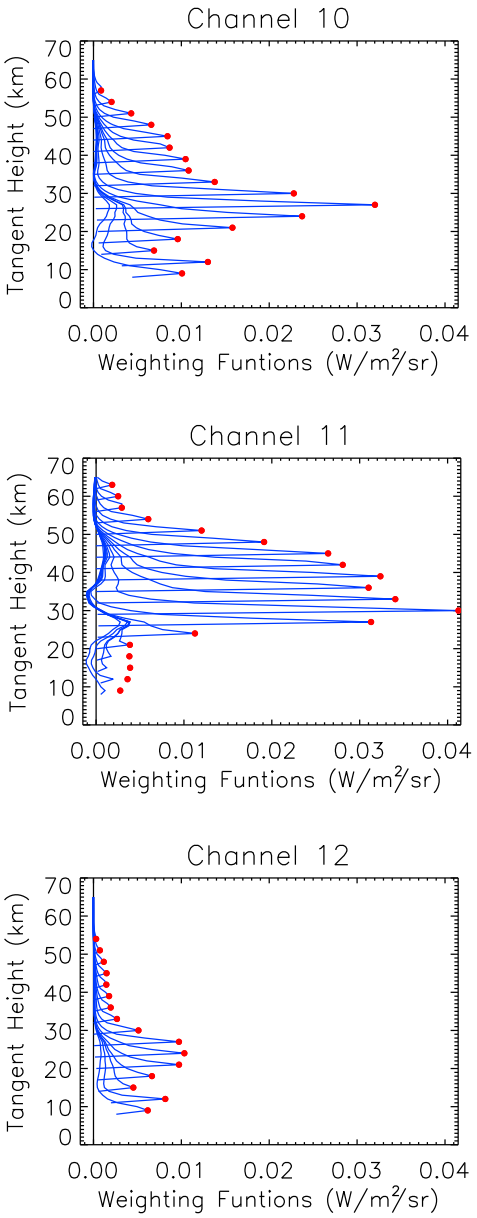

Figure 6. Weighting functions for the HIRDLS ozone sounding channels. Each curve for channel n (n = 10, 11, 12) is a plot of row i of **K** (section 4.2) and shows $\frac{\partial \mathbf{f}_j^n}{\partial ln(O_3)_i}$, which is the response of the forward model radiance (**f**) as a function of altitude (j) due to a perturbation in log of ozone volume mixing ratio at tangent height i. See Figure 4 caption for more details.

The contribution of each error source to the total error covariance can now be obtained by deriving its individual covariance matrix. For smoothing error this is

$$\begin{aligned}\mathbf{S_s} &= \mathrm{E}\{\boldsymbol{\varepsilon}_s\boldsymbol{\varepsilon}_s^{\mathbf{T}}\} = \mathrm{E}\left\{(\mathbf{A}-\mathbf{I})(\mathbf{x_t}-\mathbf{x_a})(\mathbf{x_t}-\mathbf{x_a})^{\mathbf{T}}(\mathbf{A}-\mathbf{I})^{\mathbf{T}}\right\} \\ &= (\mathbf{A}-\mathbf{I})\mathrm{E}\left\{(\mathbf{x_t}-\mathbf{x_a})(\mathbf{x_t}-\mathbf{x_a})^{\mathbf{T}}\right\}(\mathbf{A}-\mathbf{I})^{\mathbf{T}} \\ &= (\mathbf{I}-\mathbf{A})\mathbf{S_a}(\mathbf{I}-\mathbf{A})^{\mathbf{T}} \\ &= \mathbf{G_a}\mathbf{S_a}\mathbf{G_a^T}\end{aligned}, \quad (10)$$

where E is the expectation value operator, $\mathbf{S_a}$ is the error covariance matrix of the a priori data, and $\mathbf{G_a} = \frac{\partial \mathbf{x}}{\partial \mathbf{x_a}} = \mathbf{I} - \mathbf{A} = (\mathbf{S_a^{-1}} + \mathbf{K^T S_y^{-1} K})^{-1}\mathbf{S_a^{-1}}$ represents the sensitivity of the retrieved state with respect to the a priori state (the a priori gain matrix) [*Lambert et al.*, 1999]. The contributions of the other error sources are similarly derived,

$$\mathbf{S_B} = \mathrm{E}\{\boldsymbol{\varepsilon}_b\boldsymbol{\varepsilon}_b^{\mathbf{T}}\} = \mathbf{G_y}\mathbf{K_b}\mathbf{S_b}\mathbf{K_b^T}\mathbf{G_y^T}, \quad (11)$$

where $\mathbf{S_b} = \mathrm{E}\{(\mathbf{b_t}-\mathbf{b})(\mathbf{b_t}-\mathbf{b})^{\mathbf{T}}\}$ is the error covariance of model parameters,

$$\mathbf{S_F} = \mathrm{E}\{\boldsymbol{\varepsilon}_f\boldsymbol{\varepsilon}_f^{\mathbf{T}}\} = \mathbf{G_y}\mathbf{S_f}\mathbf{G_y^T}, \quad (12)$$

where $\mathbf{S_f} = \mathrm{E}\{\Delta\mathbf{f}\Delta\mathbf{f}^{\mathbf{T}}\}$ is the forward model error covariance, and

$$\mathbf{S_m} = \mathrm{E}\{\boldsymbol{\varepsilon}_m\boldsymbol{\varepsilon}_m^{\mathbf{T}}\} = \mathbf{G_y}\mathbf{S_y}\mathbf{G_y^T}, \quad (13)$$

where $\mathbf{S_y} = \mathrm{E}\{\boldsymbol{\varepsilon}_y\boldsymbol{\varepsilon}_y^{\mathbf{T}}\}$ is the covariance of measurement (radiometric) noise. Therefore, the total solution covariance can now be obtained,

$$\mathbf{S_x} = \mathbf{S_s} + \mathbf{S_B} + \mathbf{S_F} + \mathbf{S_m}. \quad (14)$$

In version 4 of HIRDLS retrievals, the input error covariance matrices (e.g., $\mathbf{S_a}$, $\mathbf{S_y}$) are constructed as shown in Table 3. Note that in this version, the a priori and forward model errors are independent of altitude, and the measurement noise is a combination of detector noise and pointing jitter error (radiance uncertainty due to imprecise pointing, smaller than detector noise by 1 to 2 orders of magnitude, depending on channel and altitude). Also, the model parameter and forward model errors are combined in a single "forward model" covariance matrix, $\mathbf{S_{f'}}$, which replaces $\mathbf{S_f}$ in equation (12) and eliminates $\mathbf{S_B}$, so that the total error is

$$\mathbf{S_x} = \mathbf{S_s} + \mathbf{S_{F'}} + \mathbf{S_m}, \quad (15)$$

where $\mathbf{S_{F'}} = \mathbf{G_y}\mathbf{S_{f'}}\mathbf{G_y^T}$.

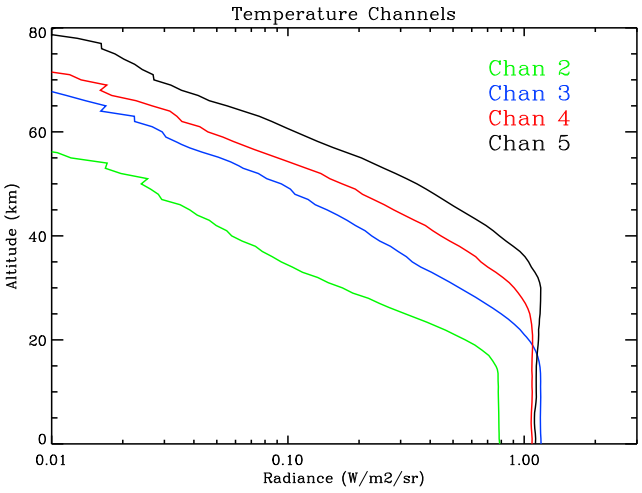

Figure 7. Variation of HIRDLS radiances with altitude in the temperature channels for the radiance scan described in Figure 1.

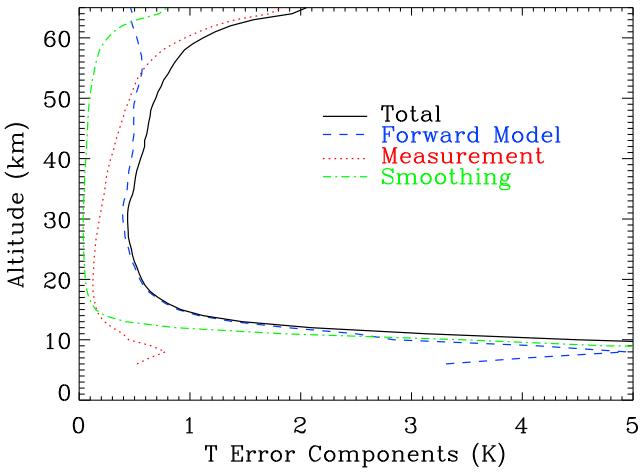

Figure 8. Components of the predicted temperature retrieval error for the 15 January 2007 radiance scan used in Figure 1 (V004, at 45.4°N; cloud top height of 9 km).

[43] An example of the above error characterization is presented in Figure 8, which shows the error decomposition for the temperature profile corresponding to Figures 1 and 4. The total error is dominated by the forward model error in the altitude range 12–40 km, with measurement (radiometric) error being the second largest component in the stratosphere. Above 40 km, contribution of measurement error increases and becomes the largest component in the lower mesosphere. The smoothing error is very small (<0.1 K) from the tropopause to the stratopause, increasing in the lower mesosphere to about 0.8 K at 65 km, where its contribution remains significantly smaller than the measurement error. This is consistent with the red curve in Figure 1 for T, which shows that the retrieval is mostly independent of the a priori in the 12–65 km range. Below 12 km, the a priori contribution to the retrieved T profile begins to increase as a consequence of decrease in radiance sensitivity due to channel saturation (Figure 7), and it dominates the retrieval below 10 km owing to presence of clouds (sections 3.5 and 4.2). Consequently, the smoothing error also begins to increase below 12 km and dominates the total error below 10 km. Note that the

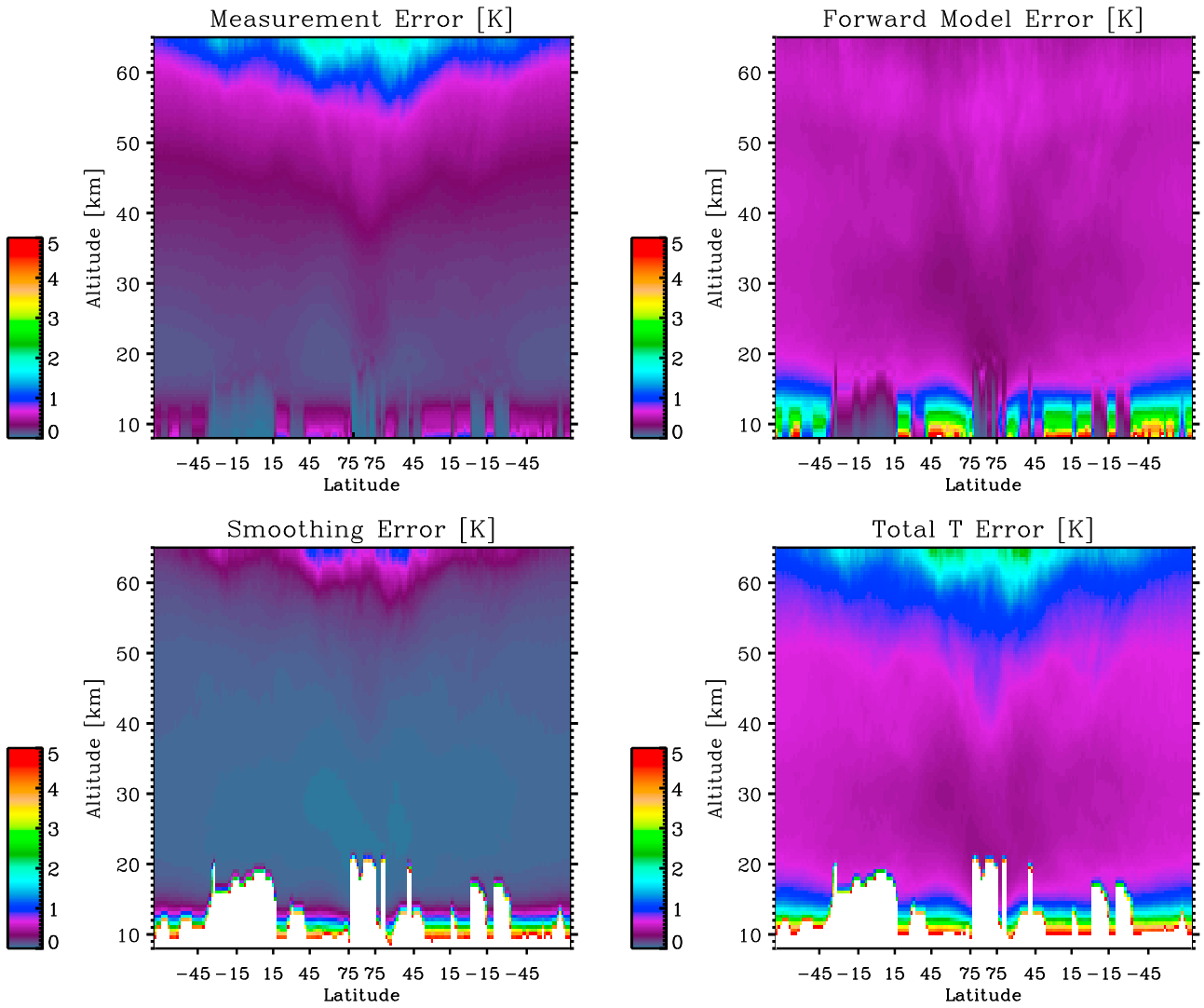

Figure 9. Maps of the components of the predicted total temperature error around the same orbit as in Figure 2. The white intrusions represent cloudy regions.

saturation heights as well as cloud top levels vary with latitude.

[44] These error characteristics generally hold for all latitudes, as illustrated in Figure 9, which shows maps of the temperature error components along a full orbit of HIRDLS retrievals. The total error is dominated by the forward model error in the upper troposphere and almost all of the stratosphere, and by the measurement error in the lower mesosphere. The smoothing error contributions become significant below about 12 km for clear sky regions, and are the dominant components in cloudy regions (white intrusions).

6. Summary and Data Status

6.1. Summary

[45] We have described the HIRDLS retrieval algorithm, which is based on the Optimal Estimation formalism of *Rodgers* [2000]. It minimizes a cost function that is constrained by the prior knowledge of the atmosphere, weighted by its covariance, to obtain vertical profiles of the desired atmospheric constituents that are consistent with the radiances calculated by the algorithm's radiative transfer model. The technique used to solve the resulting iteration equation is a modified version of the Leveberg-Marquardt approach, in which the step size, γ, is updated on the basis of the ''trust region'' concept (section 2.2).

[46] The retrievals are characterized for a northern hemisphere winter, midlatitude profile (V004 data), showing high vertical resolution of about 1–1.1 km (sharply peaked averaging kernels) and minimal a priori contribution, except in cloudy regions and at tangent heights where the channel radiances saturate. The weighting functions are relatively broad in these regions of low radiance sensitivity, but are otherwise narrow and show good response to temperature or gas mixing ratio perturbations. Curtain plots show that the characteristics of high vertical resolution and negligible a priori contribution are maintained for all latitudes along HIRDLS orbits.

[47] The total temperature error, calculated by the retrieval algorithm, varies from 0.5 K to 0.8 K from the upper troposphere to the stratopause region, consistent with the empirical estimates given by *Gille et al.* [2008]. Contributions to the total error are by measurement (detector and pointing jitter), forward model, and smoothing. In regions of strong SNR, forward model error is the largest component of the calculated temperature error, followed by measurement and smoothing errors (very small contribution). In the lower to upper troposphere regions, where clouds are present or where radiance sensitivity is low, smoothing error is the largest component, followed by forward model and measurement errors. In the upper stratosphere lower mesosphere region, the total temperature error is dominated by the measurement error. These relative weightings of the error components hold for all latitudes along HIRDLS orbits.

[48] Accuracies of the retrieved data are described in detail in the validation papers [*Gille et al.*, 2008; *Massie et al.*, 2007; *Nardi et al.*, 2008; *Coffey et al.*, 2008; *Kinnison et al.*, 2008]. As a quick reference, temperature accuracy is ±0.5 K from 400 to 10 hPa (compare sondes), and ±1 K from 10 to 1 hPa (compare ECMWF). O_3 accuracy is 20–5% from 250 to 200 hPa, and 10–1% from 200 to 5 hPa.

6.2. Data Status

[49] Correction algorithms for removing the blockage signal from the measured radiances have made possible the validation, release, and scientific applications of HIRDLS T, O_3, HNO_3, CFC-11, CFC-12, aerosol extinction at 12.1 μm, and cloud top pressure data. The latest version of these data (as of June 2009) is V004, released to the GES DISC (http://daac.gsfc.nasa.gov) in August 2008. Useful range, screening criteria, predicted retrieval error, and accuracy of the data are described in the data quality document that is also available from the GES DISC.

[50] **Acknowledgments.** We thank the following colleagues for their contributions to the HIRDLS L2 algorithm and/or other aspects of the HIRDLS program: Phil Arter (deceased), Paul Bailey, Charles Cavanaugh, Jim Craft, Alan Darbyshire, Vince Dean, Mike Dials, David Ellis, Jim Hannigan, Craig Hartsough, Linda Henderson, Brian Johnson, Doug Kinnison, Aaron Lee, Joanne Loh, Larry Lyjack, Joe Moorhouse, Soji Oduleye, Dan Packman, Chris Palmer, Dan Peters, Brent Petersen, Laurie Rokke, Leslie Smith, Brendan Torpy, Barbara Tunison, Peter Venters, Jinxue Wang, Bob Watkins, Bob Wells, John Whitney, Doug Woodard (deceased), Helen Worden, Greg Young, and Valery Yudin. In addition, Alyn Lambert would like to thank the following colleagues for their valuable comments and suggestions: Anu Dudhia, Clive Rodgers, Paul Morris, Nathaniel Livesey, and Don Grainger. We would also like to thank the reviewers of this paper for their time and constructive comments and suggestions. This work was funded by NASA's Aura satellite program under HIRDLS contract NAS5–97046. The National Center for Atmospheric Research is sponsored by the National Science Foundation. Work at the Jet Propulsion Laboratory, California Institute of Technology, was carried out under a contract with NASA.

References

Alexander, M. J., et al. (2008), Global estimates of gravity wave momentum flux from High Resolution Dynamics Limb Sounder (HIRDLS) observations, *J. Geophys. Res.*, *113*, D15S18, doi:10.1029/2007JD008807.

Bowman, K. W., et al. (2006), Tropospheric emission spectrometer: Retrieval method and error analysis, *IEEE Trans. Geosci. Remote Sens.*, *44*, 1297–1307, doi:10.1109/TGRS.2006.871234.

Carslaw, K. S., B. Luo, and T. Peter (1995), An analytic expression for the composition of aqueous HNO_3–H_2SO_4 stratospheric aerosols including gas phase removal of HNO_3, *Geophys. Res. Lett.*, *22*(14), 1877–1880, doi:10.1029/95GL01668.

Coffey, M., et al. (2008), Airborne Fourier transform spectrometer observations in support of EOS Aura validation, *J. Geophys. Res.*, *113*, D16S42, doi:10.1029/2007JD008833.

Curtis, A. R. (1952), Discussion of 'A statistical model for water vapour absorption' by R. M. Goody, *Q. J. R. Meteorol. Soc.*, *78*, 638–640, doi:10.1002/qj.49707833820.

Deeter, M. N., D. P. Edwards, and J. C. Gille (2007), Retrievals of carbon monoxide profiles from MOPITT observations using lognormal a priori statistics, *J. Geophys. Res.*, *112*, D11311, doi:10.1029/2006JD007999.

Edwards, D. P. (1992), GENLN2: A general line-by-line atmospheric transmittance and radiance model, Version 3 description and users guide, *NCAR Rep. NCAR/TN-367+STR*, Natl. Cent. for Atmos. Res., Boulder, Colo.

Edwards, D. P., J. C. Gille, P. L. Bailey, and J. J. Barnett (1995), Selection of sounding channels for the High Resolution Dynamics Limb Sounder, *Appl. Opt.*, *34*, 7006–7018.

Fleming, E., S. Chandra, J. Barnett, and M. Corney (1990), Zonal mean temperature, pressure, zonal wind and geopotential height as functions of latitude, *Adv. Space Res.*, *10*, 11–53. (Available at http://badc.nerc.ac.uk/data/cira/), doi:10.1016/0273-1177(90)90386-E.

Francis, G. L., D. P. Edwards, A. Lambert, C. M. Halvorson, J. M. Lee-Taylor, and J. C. Gille (2006), Forward modeling and radiative transfer for the NASA EOS-Aura High Resolution Dynamics Limb Sounder (HIRDLS) instrument, *J. Geophys. Res.*, *111*, D13301, doi:10.1029/2005JD006270.

Gille, J. C., and J. M. Russell (1984), The Limb Infrared Monitor of the Stratosphere: Experiment, description, performance, and results, *J. Geophys. Res.*, *89*, 5125–5140, doi:10.1029/JD089iD04p05125.

Gille, J. C., J. J. Barnett, J. C. Whitney, M. A. Dials, D. M. Woodard, W. Rudolf, A. Lambert, and W. Mankin (2003), The High Resolution Dynamics Limb Sounder (HIRDLS) experiment on Aura, *Proc. SPIE Int. Soc. Opt. Eng.*, *5152*, 162–171, doi:10.1117/12.507657.

Gille, J. C., et al. (2008), The High Resolution Dynamics Limb Sounder (HIRDLS): Experiment overview, recovery and validation of initial temperature data, *J. Geophys. Res.*, *113*, D16S43, doi:10.1029/2007JD008824.

Kinnison, D. E., et al. (2007), Sensitivity of chemical tracers to meteorological parameters in the MOZART-3 chemical transport model, *J. Geophys. Res.*, *112*, D20302, doi:10.1029/2006JD007879.

Kinnison, D. E., et al. (2008), Global observations of HNO_3 from the High Resolution Dynamics Lim Sounder (HIRDLS): First results, *J. Geophys. Res.*, *113*, D16S44, doi:10.1029/2007JD008814.

Lambert, A., P. L. Bailey, D. P. Edwards, J. C. Gille, B. R. Johnson, C. M. Halvorson, S. T. Massie, and K. A. Stone (1999), HIRLDS level-2 algorithm theoretical basis document, report, 109 pp., NASA Goddard Space Flight Cent., Greenbelt, Md. (Available at http://eospso.gsfc.nasa.gov/eos_homepage/for_scientists/atbd/docs/HIRDLS/ATBD-HIR-02.pdf)

Livingston, J. M., and P. B. Russell (1989), Retrieval of aerosol size distribution moments from multi-wavelength particulate extinction measurements, *J. Geophys. Res.*, *94*, 8425–8433, doi:10.1029/JD094iD06p08425.

Massie, S., et al. (2007), High Resolution Dynamics Limb Sounder observations of polar stratospheric clouds and subvisible cirrus, *J. Geophys. Res.*, *112*, D24S31, doi:10.1029/2007JD008788.

Nardi, B., et al. (2008), Initial validation of ozone measurements from the High Resolution Dynamics Limb Sounder, *J. Geophys. Res.*, *113*, D16S36, doi:10.1029/2007JD008837.

Olsen, M. A., A. R. Douglas, P. A. Newman, J. C. Gille, B. Nardi, V. A. Yudin, D. E. Kinnison, and R. Khosravi (2008), HIRDLS observation and simulation of a lower stratospheric intrusion of tropical air to high latitudes, *Geophys. Res. Lett.*, *35*, L21813, doi:10.1029/2008GL035514.

Rodgers, C. D. (1976), Retrieval of atmospheric temperature and composition from remote measurements of thermal radiation, *Rev. Geophys.*, *14*, 609–624, doi:10.1029/RG014i004p00609.

Rodgers, C. D. (1990), Characterization and error analysis of profiles retrieved from remote sounding measurements, *J. Geophys. Res.*, *95*, 5587–5595, doi:10.1029/JD095iD05p05587.

Rodgers, C. D. (2000), *Inverse Methods for Atmospheric Sounding: Theory and Practice*, World Sci., Hackensack, N. J.

Rodgers, C. D., R. J. Wells, R. G. Grainger, and F. W. Taylor (1996), Improved stratospheric and mesospheric sounder validation: General approach and in-flight radiometric calibration, *J. Geophys. Res.*, *101*, 9775–9793, doi:10.1029/95JD02466.

Russell, P. B., and M. P. McCormick (1989), SAGE II aerosol data validation and initial data use: An introduction and overview, *J. Geophys. Res.*, *94*, 8335–8338, doi:10.1029/JD094iD06p08335.

Schoeberl, M. R., et al. (2006), Overview of the EOS Aura mission, *IEEE Trans. Geosci. Remote Sens.*, *44*, 1066–1074, doi:10.1109/TGRS.2005.861950.

Weinreb, M. P., and A. C. Neuendorffer (1973), Method to apply homogeneous-path transmittance models to inhomogeneous atmospheres, *J. Atmos. Sci.*, *30*, 662–666, doi:10.1175/1520-0469(1973)030<0662:MTAHPT>2.0.CO;2.

J. Barnett and C. Hepplewhite, Department of Physics, University of Oxford, Oxford OX1 3PU, UK.

M. Coffey, C. Craig, D. Edwards, G. Francis, J. Gille, C. Halvorson, R. Khosravi, S. Massie, J. McInerney, and B. Nardi, Atmospheric Chemistry Division, National Center for Atmospheric Research, P.O. Box 3000, Boulder, CO 80307, USA. (Rashid@ucar.edu)

T. Eden, Computational Physics, Inc., Boulder, CO 80301, USA.

C. Krinsky, Center for Limb Atmospheric Sounding, University of Colorado, Boulder, CO 80301, USA.

A. Lambert, Jet Propulsion Laboratory, California Institute of Technology, Pasadena, CA 91109, USA.

K. Stone, ERT Corporation, Aurora, CO 80011, USA.